Catalytic Open–circuit Passivation by Thin Metal Oxide Films of p-Si Anodes in Aqueous Alkaline Electrolytes

Catalytic Open-circuit Passivation by Thin Metal Oxide Films of p-Si Anodes in Aqueous Alkaline Electrolytes

Harold J. Fu[a], Pakpoom Buabthong[b], Zachary P. Ifkovits[a], Weilai Yu[a], Bruce S. Brunschwig[c], Nathan S. Lewis[a,c]

[a]Division of Chemistry and Chemical Engineering, 127-72, California Institute of Technology, Pasadena, CA 91125, USA

[b]Division of Engineering and Applied Sciences, California Institute of Technology, Pasadena, CA 91125

[c]Beckman Institute Molecular Materials Resource Center, California Institute of Technology, Pasadena, CA 91125, USA

*Correspondence to: nslewis@caltech.edu, bsb@caltech.edu

Abstract:

Ni and NiO_x-based protective thin films are shown to catalyze the oxidation of Si in the

presence of O_2 in strongly alkaline KOH(aq) even in the absence of illumination. The O_2 in

solution drove the open-circuit potential of the electrode to > 0.4 V, which is positive of the Si

passivation potential. The elevated electrochemical potential of the surface allowed formation of

passive oxides on exposed Si regions of Si/Ni electrodes. Catalytic passivation of Si extended the

durability of an np^+-Si(100)/NiO_x photoanode to > 400 h while operating under simulated

day/night cycles. In contrast, electrodes without a Ni(O_x) layer and/or without O_2 in solution

displayed direct etching of the Si and corrosion pitting during non-illuminated, simulated

nighttime episodes of day/night cycling. The O_2-derived catalyzed passivation of Si using thin

films can be generalized to multiple phases of NiO_x as well as to materials other than Ni.

Relative to operation in aqueous alkaline conditions, decreasing the pH of the electrolyte

decreased the dissolution rate of the protective oxide layer formed by the catalyzed passivation

process, and consequently increased the durability of the photoanode, but yielded lower

photoelectrode fill factors for water oxidation due to the relatively large kinetic overpotentials

for the electrocatalyzed oxygen-evolution reaction at near-neutral pH.

Broader context:

Generating fuels from sunlight electrochemically allows for the storage and utilization of

solar energy. Electrode stability is a key consideration for photoelectrochemical solar fuels

devices. Protective coatings can enhance the durability of photoanodes under continuous

illumination, but pinholes or other defects in the protective film can expose the underlying

semiconducting light absorber to the electrolyte solution. Thus, materials that undergo corrosion

by dissolution and pitting when in contact with the electrolyte will inevitably suffer catastrophic device failure. However, materials that form passive oxide layers can facilitate self-healing at pinholes and enable continued operation as photoanodes. We describe herein a catalytic passivation process that inhibits corrosive dissolution at exposed regions of Si photoanodes by inducing the formation of a self-limiting passivating oxide layer through the O_2-derived oxidation of the Si surface catalyzed by metals or metal oxides. Understanding and generalizing this self-healing effect will inform device design so that solar fuels devices can operate with enhanced stability and efficiency when subjected to cycling between the presence and absence of sunlight.

Introduction:

Small band gap photoanodes used for water oxidation under illumination are thermodynamically unstable in strongly alkaline or acidic solution.[1, 2] However, protective coatings such as amorphous TiO_2, Ni, NiO_x, and CoO_x have extended the operational lifetime of a variety of such photoanodes including Si, GaAs, GaP, CdTe, and $BiVO_4$ for the light-driven oxygen-evolution reaction (OER) in strongly alkaline electrolytes.[3-8] Nonetheless, pinholes and other defects in the protective films can facilitate corrosion of exposed regions of the semiconductor and lead to eventual device failure.[9, 10] Common failure modes of unprotected regions are the formation of an insulating interfacial layer, generally an oxide, or corrosion that leads to pit formation that can spread through the entire photoelectrode material.

During O_2 evolution, bare Si photoanodes grow an oxide (SiO_x) passivation layer that resists corrosion and is thus resilient to pinholes in the protection layer.[11, 12] In the dark at open circuit, however, when the electrode is poised at the rest potential, the SiO_x slowly dissolves in alkaline media, in which Si itself rapidly etches. This process can lead to electrode failure under day/night cycling conditions.[6, 13, 14]

The etch rate of SiO_x is orders of magnitude slower than that of Si in alkaline solution, so the dissolution of Si in the absence of illumination can in principle be inhibited if the oxide layer can be maintained on the Si surface.[15, 16] Kinetic passivation of the Si thus occurs when the growth rate of SiO_x exceeds its rate of dissolution. The addition of $[Fe(CN)_6]^{3-}$ to a strongly alkaline solution has been shown to limit the degradation of a Si photoanode decorated with an array of Ni islands.[17] The $[Fe(CN)_6]^{3-}$ ($E^0 \sim 0.36$ V vs the normal hydrogen electrode, NHE, for $[Fe(CN)_6]^{3-/4-})$[18] sets the surface potential of the Si to be ~ 1.4 V vs the reversible hydrogen electrode (RHE), driving the formation of oxide on exposed regions of the Si surface.

Consequently, regions of the Si that are exposed to the electrolyte between the Ni islands, or even under a porous Ni oxy-hydroxy film, are inhibited from corrosion and dissolution due to the formation of the protective, passivating oxide (Scheme Ia). The durability of such interfaces is then limited by the rate of dissolution of the Si oxide in the electrolyte of interest.

np$^+$- and p$^+$-Si electrodes decorated with arrays of 3-6 μm diameter Ni islands have been reported to exhibit extended stability (> 24 h) in dark, open-circuit conditions and in the absence of protective electrolytes, even when > 80% of the Si surface is exposed to the alkaline electrolyte.[13, 17] An understanding of the chemical and spatial details of the failure processes of Si photoanodes and of the fundamental reasons why unprotected Si photoanodes do not readily fail by corrosion could provide a basis for strategies to extend the operational lifetimes of photoanodes.

Herein we have investigated the mechanism by which Si can exhibit extended operation for water oxidation under day/night cycling in alkaline electrolytes as well as under other conditions where Si would be expected to rapidly etch and undergo pit corrosion. A hypothesis is that the presence of O_2, along with an oxygen catalyst or a protective layer that can react with O_2, produces a surface potential that drives formation of Si oxide. This process (Scheme Ib) is analogous to that of a protective one-electron redox-active oxidant in the electrolyte. We demonstrate that metal or metal oxide thin films such as Ni or NiO_x, in the presence of O_2, catalyze the dark, passive oxidation of Si in alkaline electrolytes. Such films can additionally induce local oxidation of exposed Si at pinholes or other film defects and thus lead to inherent defect tolerance of such interfaces. The catalyzed passivation of Si using Ni or NiO_x thin films is thus compatible with previous investigations of Si/Ni-based photoanodes that were only evaluated under constant illumination. This behavior provides a strategy for extending the

stability of photoelectrodes at exposed regions during periods when the surfaces would otherwise be subject to etching and/or associated corrosion at pinholes in protection layers.[4, 5]

Results

Passivation and etching behavior of Si in KOH solution

Fig. 1 shows the voltammetric behavior of p^+-Si(100) electrodes between -0.1 and 1.3 V vs RHE in nominally 1 M KOH(aq) that had been saturated with 1 atm of either $O_2(g)$ or $N_2(g)$. The peaks of the anodic current at 0.17 V and 0.25 V vs RHE for O_2-saturated and N_2-saturated Si samples, respectively, correspond to the passivation potential, E_{PP}. The decrease in current at potentials positive of E_{PP} indicates the formation of a passivating surficial Si oxide.[19]

The dissolution rate, r_D, of p^+-Si(100) in 1 M KOH(aq) at open circuit (~ -0.1 V vs RHE) was $r_D > 10^2$ nm h^{-1} at room temperature.[17] Fig. S1 (ESI†) shows r_D as a function of the electrode potential. r_D at a given potential was determined by etching exposed Si on an electrode patterned with a thermal oxide mask in 1 M KOH(aq), followed by removing the mask using buffered oxide etch, and finally measuring the resulting trench height using atomic force microscopy (Fig. S1c, ESI†). The rate decreased to 71.6 nm h^{-1} at 0.2 V vs RHE and decreased further to a minimum of 1.7 nm h^{-1} at 0.5 V vs RHE, consistent with the formation of a slowly dissolving SiO_x layer at these potentials.[20] The dissolution rate increased monotonically as the potential was increased to > 0.5 V vs RHE. Over the entire potential range, $r_D(E)$ correlated closely with the current density at the potential, E, of interest (Fig. S1b, ESI†). At low (< 2 V) applied voltages, the Si dissolution behavior is consistent with expectations for a surface covered by a potential-dependent, steady-state thickness of Si oxide.[21]

Catalyzed passivation of p^+-Si by Ni in O_2-saturated strongly alkaline KOH(aq)

The morphology of etched Si(100) in KOH solution was used to provide information on the mechanism of the potential-dependent Si etching in the presence of various catalysts and surface layers.[22] In 1 M KOH(aq), the Si(100) facets etch more rapidly than the Si(111) facets, leading to the formation of inverted pyramid-shaped pits on the Si(100) surface.[10, 19, 23] Conversely, the SiO$_x$ passivation layer etches isotropically but at a rate < 0.1 times that of Si, leading to facet-independent circular etch pits on oxide-covered Si surfaces.[15, 17]

Fig. 2 displays the open-circuit etching behavior of p$^+$-Si(100), of p$^+$-Si(100) with a thin film of 5 nm Ni (p$^+$-Si(100)/Ni), and of p$^+$-Si(100) with 60 nm of NiO$_x$ (p$^+$-Si(100)/NiO$_x$) in strongly alkaline 1 M KOH(aq) saturated with 1 atm of either O$_2$(g) or N$_2$(g). Electrodes tested in N$_2$-saturated solution were used as a control during which O$_2$ was purged from the cell. Unless otherwise stated, all of the films on Si were deposited as continuous thin films. Bare p$^+$-Si(100) electrodes, in O$_2$- or N$_2$-saturated solutions, had open-circuit potentials, E_{oc}, $< E_{PP}$ with average potentials of E_{oc} = -0.07 and -0.11 V vs RHE (i.e. more than 0.2 V negative of E_{PP}). This low E_{oc} implies the direct dissolution of Si at open circuit regardless of whether O$_2$ is present in the solution. In N$_2$-saturated solution, p$^+$-Si(100)/Ni or p$^+$-Si(100)/NiO$_x$ surfaces initially exhibited E_{oc} ~ 0.6 vs RHE and E_{oc} ~ 1.0 V vs RHE, respectively; however, within a few hours the E_{oc} of both surfaces decreased to < 0 V vs RHE (Fig. 2b). In contrast, in O$_2$-saturated solution, p$^+$-Si(100)/Ni or p$^+$-Si(100)/NiO$_x$ surfaces exhibited E_{oc} > 0.60 and > 0.85 V vs RHE, respectively, throughout the duration of the experiment (Fig. 2a).

The resulting etched electrode surfaces were characterized using scanning electron microscopy (SEM). After 120 h at open circuit in the O$_2$-saturated electrolyte, SEM images of the p$^+$-Si(100)/Ni surface showed circular etch pits (Fig. 2c). In contrast, after only 20 h at open-circuit in the N$_2$-saturated electrolyte (Fig. 2d, inset) p$^+$-Si(100)/Ni surfaces displayed inverted

pyramids that visibly undercut the Ni film. Further, after 120 h continued undercutting led to a merging of the Si etch pits with the complete delamination of the Ni film on p^+-Si(100)/Ni surfaces under N_2, as confirmed by energy-dispersive X-ray spectroscopy (EDS, Fig. S2, ESI†). Qualitatively similar open-circuit etching behavior was also observed for p^+-Si(100)/NiO$_x$ electrodes in either O_2- or N_2-saturated solutions (Fig. S3, ESI†). The cross section of the sample saturated in O_2 showed that the underlying Si remained intact (Fig. S3c, ESI†).

To further investigate the potential-dependent behavior of the etching of Si electrodes, a p^+-Si(100)/Ni electrode was held at $E = -0.1$ V vs RHE in O_2-saturated 1 M KOH(aq). After 20 h, SEM images showed inverted pyramids undercutting the Ni film (Fig. S4, ESI†), similar to the behavior of a p^+-Si(100)/Ni sample in a N_2-saturated solution.

Fig. S5 (ESI†) shows E_{oc} as a function of the thickness of the Ni film on p^+-Si(100)/Ni electrodes in O_2- and N_2-saturated 1 M KOH(aq). In O_2-saturated solutions, all electrodes showed initial values of E_{oc} between 0.7 and 0.8 V vs RHE. E_{oc} remained in this range for the first hour, but after 120 h, E_{oc} was 0.29, 0.60, 0.64, and 0.73 V vs RHE for 3 nm, 5 nm, 30 nm, and 60 nm thick Ni films on p^+-Si(100), respectively. Fig. S6 (ESI†) shows SEM images of these electrodes after 120 h at open circuit in O_2-saturated 1 M KOH(aq). Pronounced and spatially dense pinholes were produced on the p^+-Si(100)/Ni electrode that had 3 nm of Ni, whereas the pinhole density decreased with increasing Ni thickness. The p^+-Si(100)/Ni electrode with 60 nm of Ni exhibited much less undercutting of Ni. Regardless of the Ni film thickness, in N_2-saturated 1 M KOH(aq), E_{oc} for the p^+-Si/Ni electrodes decreased to $< E_{PP}$ within a few h of immersion, with 3 nm, 5 nm, and 30 nm thick Ni films requiring 1.6 h, 2.3 h, and 3.3 h, respectively, to produce $E_{oc} < 0.2$ V vs RHE (Fig. S5b, ESI†).

Fig. S7 (ESI†) shows the behavior in O_2-saturated 1 M KOH(aq) of p^+-Si(100) electrodes

coated with discrete, patterned Ni islands (µNi). A p^+-Si electrode patterned with an array of 60 nm thick, 3 µm diameter Ni islands (µNi) with a 7 µm pitch, p^+-Si(100)/(µNi), exhibited a relatively steady potential of E_{oc} = 0.6 V vs RHE for ~ 120 h. Despite ~ 86% of the Si surface being exposed to the electrolyte, the electrode did not exhibit characteristics of direct Si etching in the absence of illumination. In fact, SEM images showed no signs of inverted pyramid formation after the 120 h experiment, and the µNi array remained intact with minor radial undercutting (~ 300 nm) of the µNi islands. The etching of the exposed Si surface was similar to the behavior exhibited by a Si/µNi electrode passivated in KOH(aq) that contained a protective electrolyte.[17]

Fig. S8 (ESI†) compares the electrochemical behavior of p^+-Si/NiO$_x$ electrodes in O$_2$- or N$_2$-saturated 1 M KOH(aq). The E_{oc} of electrodes was measured for 6 h in 1 M KOH(aq), followed by chronoamperometry (CA) at 0.3 V vs RHE for 1 h, after which cyclic voltammetry (CV) was performed from E_{oc} to +0.4 to -0.4 V vs E_{oc} at 10 mV s^{-1}. This cycle was repeated three times. At a potential that is positive of E_{PP}, 0.3 V vs RHE, reductive current was observed in both O$_2$-saturated and N$_2$-saturated solutions (Fig. S8b, ESI†).

As-deposited Ni films exhibit a relatively high overpotential for the OER in 1 M KOH(aq), in contrast to Fe-doped, Ni oxy-hydroxy (NiFeOOH) films.[24] Fig. 3 compares the open-circuit potentials in 1 M KOH(aq) for p^+-Si(100) electrodes coated with either Ni or NiFeOOH films. Ni was converted to NiFeOOH by cycling the electrode potential between 0.3 and 1.63 V vs RHE at 40 mV s^{-1} in 1 M KOH(aq) to oxidize the Ni and incorporate residual Fe from the solution.[25] In both O$_2$- and N$_2$-saturated 1 M KOH(aq), p^+-Si(100)/NiFeOOH electrodes initially displayed E_{oc} = 0.96 V vs NHE, but E_{oc} decreased within < 2 h of operation and converged towards E_{oc} values characteristic of as-deposited Ni films in both O$_2$- and N$_2$-saturated

solutions. For the O_2-saturated solution, $E_{oc} = 0.65$ V vs RHE after 83 h, whereas for the N_2-saturated solution, $E_{oc} = 0.07$ V vs RHE after 4.3 h. The shift in E_{oc} of the Ni film in O_2- or N_2-saturated solution can be ascribed to changes in the relative amounts of oxidized Ni on the surface. The Ni oxy-hydroxy film readily converts to Ni oxide on the electrode surface at E_{oc},[26] because the potential for converting Ni^{II} into Ni^{III} is positive of E_{oc}, lying in a potential region of ~1.3 V vs RHE.[27]

Si passivation using other catalysts

The open-circuit potential of p^+-Si(100) electrodes coated with either Pt, Co, or TiO_2 was also evaluated in O_2-saturated KOH solution (Fig. S9, ESI†). Amorphous TiO_2 was investigated due to its ability to provide a protective layer on Si,[3, 11, 28] whereas Pt and Co were chosen due to their electrocatalytic activity for the ORR.[29-31] p^+-Si(100)/Pt electrodes displayed $E_{oc} > 0.8$ V vs RHE for 120 h, with minimal undercutting of the film (Fig. S9b, ESI†). In contrast, within a day of immersion of p^+-Si(100)/Co or p^+-Si(100)/TiO_2 surfaces, E_{oc} decreased from initial values of $E_{oc} = 0.74$ and $E_{oc} = 0.49$ V vs RHE, respectively, to < 0.25 V vs RHE. After immersion, both types of electrodes exhibited inverted pyramid etch pits (Fig. S9c-d, ESI†), indicating that despite E_{oc} being slightly (< 0.1 V) more positive than E_{PP}, the rate of Si dissolution at open-circuit was greater than the rate of Si oxidation. No apparent correlation was observed between the catalytic activity of Pt, Co, Ni, and NiO_x films for the ORR and the catalyzed passivation of Si (Fig. S10, ESI†).

Photoelectrochemical characterization of catalytically passivated Si photoanodes subjected to simulated day/night cycling

Fig. 4 depicts the photoelectrochemical performance and stability of np$^+$-Si(100)/NiO$_x$

photoanodes in 1 M KOH(aq) while undergoing cycling between 18 h intervals at open-circuit

conditions in the dark ("night") and 6 h intervals of 100 mW cm^{-2} illumination at $E = 1.63$ V vs

RHE ("day"). The photoelectrochemical cell was open to ambient air (~ 0.2 atm O$_2$) but was not

continuously purged with O$_2$. Throughout the duration of the experiment, the photoelectrode

exhibited a light-limited current density of 31.0 ± 1.5 mA cm^{-2} during the day cycle (Fig. 4a),

with small variations of photocurrent within individual day cycles consistently attributable to

differing amounts of electrochromic darkening.[32] Cyclic voltammograms collected at the

beginning of each day cycle (Fig. 4b) were also essentially unchanged throughout the

experiment. From 0 h to 114 h, the shift in potential (0.13 V shift negative at a current density of

1 mA cm^{-2}) and the increase in current density for the Ni^{III}/Ni^{II} redox peaks were consistent with

an increase in catalytically active sites exposed to the electrolyte.[6] Throughout every simulated

night cycle, E_{oc} was > 0.6 V vs RHE (Fig. 4c), indicating that the Si was coated with a

passivating oxide layer and confirming that the O$_2$ concentration in the electrolyte was sufficient

to maintain the passivating oxide. At the beginning of each simulated night cycle, E_{oc} started at $\sim$

1.3 V vs RHE and decreased to either $\sim 0.6 - 0.8$ V vs RHE in the first five night cycles or ~ 1.2

vs RHE during subsequent night cycles. The change in E_{oc} during each night cycle suggests that

the catalytically active Ni^{III} oxy-hydroxy film generated during the day likely converted to a Ni^{II}-

based oxide during the night.

After day/night cycling, SEM images revealed isotropically etched Si at pinholes in the

photoelectrode (Fig. 4d). The images revealed that the NiO$_x$ film remained intact on the Si

surface with some undercutting around the pinholes, as expected for Si/Ni electrodes in alkaline

media.[6] In the Si 2p X-ray photoelectron spectrum (XPS) of the photoelectrode surface that was

subjected to day/night cycling, a weak SiO_2 signal (102.6 eV binding energy), but no Si peak (~

99 eV), was present.[33] This behavior confirms that the exposed regions of the surface were small

areas of oxidized Si under pinholes, with the majority of the unoxidized Si being obscured by the

NiO_x film (Fig. S11, ESI†).

Under similar day/night cycling conditions, an np^+-Si/TiO$_2$/Ni photoanode in 1 M

KOH(aq) did not exhibit catalyzed passivation despite the presence of a conformal layer of Ni on

the TiO_2 film (Fig. S12, ESI†). Instead, the electrode exhibited similar open-circuit behavior to

that of p^+-Si/TiO$_2$ electrodes in the dark (Fig. S9, ESI†). Although the photoanode maintained

performance for the first 216 h of the run, from 216 h to 312 h the photocurrent density

decreased by ~ 17%. Further, the bias sufficient to produce 10 mA cm^{-2} of photocurrent density

under simulated 100 mW cm^{-2} illumination increased by 90 mV (Fig. S12c, ESI†), indicating

substantial corrosion of the underlying np^+-Si junction. Large (> 20 μm) inverted pyramid etch

pits that undercut the TiO_2/Ni film were observed by SEM after 312 h of day/night cycling (Fig.

S12d, ESI†).

Surface characterization of catalytically passivated p^+-Si/Ni and np^+-Si/NiO$_x$

Fig. 5 compares the XPS data in the Ni $2p_{3/2}$ region for as-deposited p^+-Si/Ni electrodes

to p^+-Si/Ni electrodes that had been immersed for 20 h in N$_2$-saturated 1 M KOH(aq), as well as

to p^+-Si/Ni electrodes that had been immersed for 20 h in O$_2$-saturated 1 M KOH(aq). The XPS

emission at a binding energy of 852.4±0.1 eV is associated with metallic Ni, whereas the

emissions at binding energies of 853.5±0.2 and 855.8±0.2 eV are associated with phases of NiO

and Ni(OH)$_2$.[34, 35] The presence of NiO_x peaks indicated that the oxidation of Ni proceeded at

open circuit in 1 M KOH(aq) when O$_2$ was present in solution, as suggested by the increase in

the high-energy peak shaded in light blue (Fig. 5). Alternatively, after 20 h in N$_2$-saturated 1 M

KOH(aq), the composition of the Si surface was similar to that of the as-deposited electrode. After 120 h at open circuit in O_2-saturated 1 M KOH(aq), atomic force microscopy (AFM) showed that the Ni surface morphology exhibited an increase in average surface roughness (R_a), from 0.2 to 1.8 nm, as a result of immersion in KOH(aq), and grain boundaries subsequently formed on the Ni surface (Fig. S13, ESI†). Cross-sections of the AFM illustrate the etch pit morphology caused by SiO_x dissolution (Fig. S13c, ESI†).

Fig. S14 (ESI†) shows the Ni $2p_{3/2}$ XPS data for as-deposited, np^+-Si/NiO_x photoelectrodes relative to np^+-Si/NiO_x photoelectrodes after 20 h in O_2-saturated 1 M KOH(aq) at open circuit, as well as after extended day/night stability cycling (Fig. 4). Prior to XPS measurements, the open-circuit potentials for the latter two photoelectrodes were $E_{oc} \sim 0.6$ V vs RHE and $E_{oc} \sim 1.2$ V vs RHE, respectively. The XPS emissions at binding energies of 854.0±0.2 and 855.8±0.2 eV can be attributed to NiO, Ni(OH)$_2$, and NiO(OH).[34-36] The photoelectrode held at open circuit displayed a similar Ni $2p_{3/2}$ spectrum to that of the as-deposited NiO_x film, indicating that a mix of nickel oxides was present on both surfaces. In contrast, the XPS data for the photoelectrode after extended day/night cycling revealed an emission at 855.8 eV but no lower energy emission (854.0 eV), indicating an increase after cycling of the electrode of species that had the higher oxidation state of Ni.

Operation at near-neutral pH to inhibit the rate of SiO_x dissolution

Fig. S15 (ESI†) displays the dissolution behavior of p^+-Si(100) in O_2-saturated, 0.5 M potassium borate buffer (K-Bi, pH 9.5), with the native oxide of p^+-Si electrodes removed using buffered oxide etch prior to immersing the electrode in K-Bi. Analysis of the electrolyte by inductively coupled plasma mass spectrometry (ICP-MS) showed a negligible rate of Si dissolution for electrodes held either at open circuit or at 1.63 V vs RHE (Fig. S15a, ESI†). A p^+-

Si(100) electrode that had been cycled immediately after immersion in K-Bi exhibited an anodic peak indicative of E_{PP} at 0.31 V vs RHE (Fig. S15b, ESI†). In contrast, a p^+-Si electrode that was first held for 20 h at open-circuit in K-Bi did not exhibit an anodic peak, suggesting that a self-limited oxide had formed during immersion into the electrolyte (Fig. S15b, ESI†). XPS data confirmed the presence of SiO_x after immersion of p^+-Si in KBi at open circuit for 20 h (Fig. S16, ESI†). A p^+-Si electrode that was similarly immersed in O_2-saturated 1 M KOH(aq) for 20 h did not however exhibit a SiO_2 peak in the Si 2p XPS region, indicating that Si dissolution dominated SiO_x formation in KOH solution, but a relatively stable SiO_x layer instead spontaneously formed at pH 9.5.

Fig. 6 compares the performance of an np^+-Si(100)/Ni photoanode under simulated day/night cycling in ambient (~ 0.2 atm O_2) conditions in 0.5 M K-Bi to the behavior under conditions analogous to those used for the KOH solutions. The steady light-limited photocurrent density was > 24 mA cm^{-2} throughout the duration of each 120 h experiment. In 1 M KOH(aq), the photoanode exhibited qualitatively similar E_{oc} vs time behavior to that of the np^+-Si/NiO$_x$ photoanode shown in Fig. 4, as expected due to the oxidation of surficial Ni to NiO$_x$. In contrast, in K-Bi, E_{oc} decreased from ~ 1.4 V to ~ 1.0 V vs RHE, followed by a comparatively gradual decline to E_{oc} ~ 0.7 - 0.8 V vs RHE, possibly due to a gradual conversion of Ni(Fe)OOH to NiO/Ni(OH)$_2$. The photoanode exhibited a higher fill factor in 1 M KOH(aq) than in 1.0 M K-Bi(aq), with a ~140 mV negative shift in initial onset potential and a reduction in series resistance from 15 Ω to 7 Ω as the pH was increased. These differences in performance were consistent with the increased overpotentials associated with the OER as the pH was decreased from highly alkaline conditions to near-neutral pH values.[4, 37] In both solutions, the photoanodes exhibited relatively unchanged voltammetric behavior throughout the 120 h experiment, but

substantial changes to the surface morphology were nevertheless evident. Specifically, after cycling in 1 M KOH(aq), the photoanode surface was covered with circular etch pits, whereas no etch pits were observed on the photoanode that had been cycled in 1.0 M K-Bi(aq).

Discussion

Proposed mechanism for catalytic passivation of Si using Ni-based thin films

Si passivation in alkaline media is achieved by poising the surface potential of the Si electrode sufficiently positive of E_{PP} to oxidize any exposed Si. Previous work demonstrated this passivation effect using $[Fe(CN)_6]^{3-}$ as a strong oxidant,[17] whereas this work demonstrates that a Ni-based (or other) coating is sufficient to produce this effect in O_2-saturated alkaline solution. Multiple Ni species (e.g. Ni, NiO, Ni(OH)$_2$, and NiO(OH)) are capable of passivating Si; while the specific Ni species present influences the surface potential of the Si/Ni anode, the potential remains sufficiently positive to maintain Si passivation regardless of the Ni species (Fig. 2, 3, and S3, ESI†). The formation of passive oxides on the Si surface at open circuit in O_2-saturated KOH with Ni-based coatings allows the underlying Si to be protected even if the Ni(O$_x$) film does not conformally cover the surface. For instance, 3 μm diameter μNi regions led to the passivation of regions of exposed Si that were microns away from the Ni islands (Fig. S7, ESI†).

A combination of a Ni-based thin film and O_2 in solution was required to facilitate Si passivation. Without the Ni(O$_x$) thin film, the E_{oc} of Si electrodes was ~ -0.1 V vs RHE and thus substantially below the anodic threshold for Si oxidation of $E_{PP} = 0.17$ V vs RHE (Fig. 1). At this potential, the observed inverted pyramid etch pits indicate rapid etching of Si(100) (Fig. 2d and S4, ESI†). Without O_2 in the electrolyte, a Ni(O$_x$) film can initially define the surface potential of the electrode, likely due to the NiO, Ni(OH)$_2$, and NiO(OH) species on the surface, but within a

few hours E_{oc} declined to $< E_{PP}$ and moved towards the open-circuit potential of Si (Fig. 2b).

This decline indicates that the surface potential of the electrode is ultimately defined by Si

dissolution. Conversely, Si(100) passivation in the presence of both O_2 and a $Ni(O_x)$ thin film is

evident as shown by circular etch pits caused by isotropic SiO_2 etching (Fig. 2c) and evidence of

SiO_2 at pinholes via XPS after testing (Fig. S11, ESI†).

The surface potential of the Si electrode at open circuit will equilibrate with the solution

redox potential only if the solution couple can react at the Si surface. In the case of the O_2/OH^-

(E^0 = 1.23 V vs RHE) redox couple, bare Si does not provide a low-energy pathway between the

redox species. Thus, for a p^+-Si electrode, the surface potential does not equilibrate with an O_2-

saturated 1 M KOH solution at open circuit. However, when the surface potential is controlled

by a catalyst on the surface (p^+-Si/Ni(O_x)), the potential responds to the presence of the O_2 in the

KOH(aq) solution.

The surface potential of p^+-Si/Ni(O_x) electrodes is controlled by three factors: the redox

couples within the NiO_x film; interactions with solution redox couples; and dissolution of the

bare Si. The K_{sp} of $Ni(OH)_2$ is ~ 10^{-15}, so in strongly alkaline electrolytes only trace amounts of

$Ni(aq)^{2+}$ are present and solution Ni redox couples are not important.[38] For a p^+-Si/Ni(O_x)

electrode under illumination or under anodic conditions, the Ni surface became more oxidized

(Fig. 5). However, without O_2 in the electrolyte, the Ni species on the surface of Si/Ni(O_x)

electrode did not prevent the E_{oc} from decreasing to a value close to that of a bare Si electrode,

below E_{PP} (Fig. 2). Thus, for a p^+-Si/Ni(O_x) electrode, the Ni solid-state redox couples alone did

not dominate the electrode potential relative to Si dissolution. Thus, for p^+-Si/Ni(O_x) in an O_2-

rich solution, the interactions between the Ni(O_x) on the surface of the electrode and the solution

O_2/OH^- couple define the surface potential of the Si electrode, likely involving the oxidation and reduction of Ni species on the electrode surface.

When O_2 is not present in the solution, few or no solution redox species are present. The solution potential is therefore largely undefined and cannot buffer the electrode potential despite the presence of a $Ni(O_x)$ catalytic layer. Rather, the surface potential of the electrode is largely defined by Si oxidative dissolution, and as a result, the E_{oc} of the electrode rapidly decreases to negative of E_{PP}.

The above observations suggest a correlation between the catalytic activity of the overlayer and Si passivation (Fig. S8c and S10, ESI†). This expectation is supported by the passivation of Si that was observed for p^+-Si/Pt films in O_2-saturated solutions (Fig. S9a-b, ESI†). The data are consistent with a model in which Si/Pt and Si/Ni surfaces are in communication with the O_2/OH^- solution couple. However, this simple correlation is however not observed for Si covered by Co. The behavior of the Si/Co surfaces is consistent with complete air oxidation of the Co layer resulting in an electrically nonconductive overlayer,[39] that precludes effective redox-catalyzed communication with the dissolved O_2 to maintain the surface potential of the Si positive of E_{PP}.

The Si/TiO$_2$ surface is also electrically nonconductive, and hence leads to etching of the Si.[40] The Si/TiO$_2$/Ni interface has a buried Si surface, so changes in solution potential affect the Ni but do not affect the buried Si/TiO$_2$ junction nor affect the surface potential of the Si.[41]

Assessing and mitigating SiO$_x$ dissolution

Although open-circuit Si passivation can extend device lifetimes by hundreds of hours for photoanodes subjected to day/night cycling in KOH solution,[17] the gradual dissolution of SiO$_x$

will ultimately limit the overall device lifetime.[13] Furthermore, the rate of SiO_x dissolution is influenced by the surface potential of the Si that results from day and night conditions. Given the monotonic increase of the SiO_x dissolution rate for potentials > 0.5 V vs RHE (Fig. S1a, ESI†), the day cycle when the potential is held at 1.63 V vs RHE produces a larger etch rate than the night cycle, which results in a surface potential at the rest potential for the electrode in the dark. For a Si/Ni photoanode, the open-circuit potential shifted from $E_{oc} \sim 0.7$ V vs RHE (night) to $\geq$ 1.5 V vs RHE (day) (Fig. 6c). Consequently, Si/Ni photoanodes undergoing day/night cycling exhibited more rapid SiO_x etching (Fig. 6d) than Si/Ni electrodes held at open circuit (Fig. S6b, ESI†), as shown by the 1010 ± 70 nm and 380 ± 40 nm diameter etch pits, respectively.

Several strategies have potential to further inhibit the dissolution rate of SiO_x and extend the lifetime of the oxide-coated photoanodes. In one approach, the photoanode could be held at less positive operating potentials during the day cycles. For instance, an np$^+$-Si/Ni photoanode in 1 M KOH(aq) (Fig. 6b) approaches the light-limited photocurrent density at an applied potential of ~ 1.2 V vs RHE rather than at 1.6 V vs RHE. Consequently, operating at a less positive potential during the day cycles could potentially inhibit the dissolution of the SiO_x (Fig. S1a, ESI†). The oxide grown electrochemically could potentially be post-processed to a denser, more slowly dissolving oxide by thermal treatment, or could potentially be converted chemically to more inert materials such as Si nitrides, oxynitrides, carbides, or oxycarbides.

Operating the photoelectrode at pH 9.5 can also substantially inhibit dissolution of SiO_x (Fig. S15, ESI†), although the lower pH introduces performance limitations due to increases in polarization losses and increased kinetic overpotentials for the OER. Additionally, the oxidized Ni film is partially soluble in K-Bi, and the associated loss of catalyst might consequently deleteriously reduce the device lifetime.[42] The work herein clearly provides a systematic

understanding of the durability of photoelectrodes by identifying the medium-term failure modes and mechanisms and then rationally implementing steps to mitigate the corrosion processes of concern.

Conclusions

Coating of Si with Ni or NiO_x thin films prevented rapid Si dissolution in O_2 saturated strongly alkaline electrolytes subjected to dark, open-circuit conditions. The combination of a Ni/NiO_x catalyst and O_2 in the electrolyte maintained the Si surface potential at > 0.6 V vs RHE, positive enough to catalyze the growth of SiO_x on the Si surface at a rate faster than its dissolution. The O_2 in the electrolyte plays an important role in driving the kinetics for Si passivation. Without O_2 in the electrolyte the surface potential was defined predominantly by Si dissolution (~ -0.1 V vs RHE).

An np^+-Si/NiO_x photoanode undergoing day/night cycling exhibited stable performance for > 408 h. The catalyzed passivation process reduced the rate of corrosion of exposed Si at pinholes in the NiO_x film. Catalytic passivation of Si was observed with multiple phases of Ni – Ni, NiO, $Ni(OH)_2$, and NiOOH – as well as with Pt. Although Si-based photoanodes are susceptible to eventual failure due to slow SiO_x dissolution and subsequent undercutting of the protective film, this effect can be circumvented by leveraging the thermodynamic stability of SiO_2 in pH 9.5 at the expense of an increased resistance and positive shifts in the onset potential. This work underscores the ability of well-established Si photoanode configurations to withstand rapid corrosion associated with patterns of diurnal insolation. Moreover, the work demonstrates the benefits of a systematic approach to increase the durability of photoelectrodes by identifying the dominant failure modes of the device and taking rational steps to mitigate such processes.

Experimental

Chemicals and Materials:

Unless otherwise stated, all chemicals listed were used as received, including potassium hydroxide (KOH, Macron Fine Chemicals, AR grade $\geq$ 85%), boric acid (H_3BO_3, Sigma-Aldrich, $\geq$99.5%), ammonium hydroxide (NH_4OH, EMD Millipore Co., 28.0-30.0%), hydrochloric acid (HCl, EMD Millipore Co., 36.5-38%), hydrogen peroxide (H_2O_2, EMD Millipore Co., 30%), buffered oxide etchant (BOE, 6:1 NH_4F to HF, Transene Company, Inc.), boron nitride wafers (Saint-Gobain, BN-975 PDS), and Fumasep (Fuel Cell Store). Boron-doped, (100)-oriented p^+-Si (0.001-0.005 Ω cm resistivity) and phosphorous doped, (100)-oriented n-Si (0.1-1.0 Ω cm resistivity) wafers were purchased from Addison Engineering, Inc. Ni, Co, and Pt sputtering targets were obtained from the Kurt J. Lesker Company. Tetrakis(dimethylamido)-titanium (TDMAT, Strem Chemicals) was used for atomic layer deposition (ALD). Photoresist (Shipley 1813), MCC primer 80/20 (Microchem Corp.), and MF-319 developer (Microchem Corp.) were used for photolithography. Ag paint (Ted Pella, Inc.), gallium-indium eutectic (Alfa Aesar, 99.99%), and epoxy (Loctite 9460) were used for preparation of electrodes. Deionized water with a resistivity ρ > 18.2 MΩ cm was obtained from a Barnstead Millipore purification system.

Electrode Preparation:

np^+-Si(100) photoelectrodes were fabricated via boron diffusion doping. Prior to doping, n-type Si wafers were cleaned by immersing in 5:1:1 H_2O:NH_4OH:H_2O_2 (by volume) at 75 ˚C for 15 min, followed by a 30 s etch in BOE to remove the oxide, immersing in 6:1:1 H_2O:HCl:H_2O_2 (by volume) at 75 ˚C for 15 min, and etching once more in BOE for 30 s. After

each step the wafers were rinsed with deionized water and dried under flowing $N_2(g)$. While the

wafers were being cleaned, a tube furnace used for diffusion doping was heated to 950 ˚C for 30

min under a 5 L min^{-1} flow of O_2 to oxidize the boron nitride wafers. The gas supply was

switched from O_2 to N_2 for 30 min followed by cooling to 750 ˚C. The cleaned wafers were

transferred to a tube furnace and placed a few mm from the oxidized boron nitride wafers. A p$^+$-

emitter was formed on the wafers after increasing the temperature to 950 ˚C under a 2 L min^{-1}

flow of N_2. To deglaze B_2O_3 from the surface, the sample was taken out and cooled before

submerging in BOE for 2 min. Low-temperature oxidation at 750 ˚C under 5 L min^{-1} for 30 min

was performed, followed by etching in BOE for 5 min to remove surface defects. The final sheet

resistance was ~ 70-80 Ω sq^{-1} as measured by a four-point probe (Jandel).

Ni, NiO$_x$, Pt, and Co films were deposited onto np$^+$-Si or p$^+$-Si wafers using radio-

frequency (RF) sputtering (AJA Orion sputterer). Prior to deposition, the p$^+$-Si electrodes were

cleaned and etched in BOE by the same process described above for n-type wafers. For

deposition of Ni, Co, and Pt, 100 W was applied under 20 sccm of Ar flow at a 5 mTorr chamber

pressure until the desired thickness of material was obtained. NiO$_x$ films were deposited applying

120 W to the Ni target under 20 sccm Ar and 1 sccm O_2 at 300 ˚C at a chamber pressure of 5

mTorr. The deposition rate was calibrated via profilometry (Bruker DektakXT Stylus

profilometer) of the film that had been deposited onto a glass slide. Unless otherwise stated, the

thickness of Ni, Co, and Pt were 5 nm whereas NiO$_x$ and Ni islands had thicknesses of 60 nm.

A carbide scribe was used to cleave off edges of samples from wafers, to prevent

shunting during electrochemical operation. In-Ga eutectic was scratched onto the back of each

sample and attached to Sn-coated Cu wire using Ag paint. The wire was threaded through a glass

rod and the edges of the sample were sealed to the glass using epoxy. The epoxy was cured

overnight before testing the electrode the following day. Electrode areas were determined using ImageJ software in conjunction with an optical image of the electrode surface.

Electrochemical characterization

Electrodes were electrochemically tested in a three-electrode setup. A two-compartment cell separated by a Fumasep anion-exchange membrane was used for electrochemistry in KOH solution, whereas a single compartment cell with the catholyte separated from the anolyte by a fritted glass tube was used for electrochemistry in 0.5 M K-borate buffer (K-Bi). Nominally 1 M KOH solutions were prepared by dissolving 56.0 g of hydrated KOH pellets into a total final volume of 1 L of deionized water, with the resulting pH measured as ~13.6.[43] K-Bi was prepared by mixing 1.0 M H_3BO_3(aq) and 0.5 M KOH(aq). The anolyte side of the cell was filled with 25 mL of electrolyte and the catholyte was filled to match the liquid height in the anolyte. Either O_2 or N_2 gas was bubbled into the anolyte as appropriate. A Hg/HgO reference electrode was used in KOH(aq) and a saturated calomel electrode (SCE) was used in K-Bi(aq). Reference electrodes were calibrated relative to the RHE using a Pt disk electrode in the respective electrolyte that was continually saturated with H_2. The Hg/HgO and SCE electrodes had potentials in the range of 0.908 - 0.920 V vs RHE and 0.772 - 0.785 vs RHE, respectively, in 1 M KOH(aq) and 0.5 M K-Bi(aq), respectively. Ni wire was used as the counter electrode and was in contact with the catholyte. A MPG-2 potentiostat (Bio-Logic Science Instruments) was used for electrochemical measurements. For working electrodes using Ni as an OER catalyst, the film was initially activated via cyclic voltammetry by cycling 20 times between 0.63 and 1.63 V vs RHE in KOH solution at 40 mV s^{-1} to incorporate Fe from solution and form NiFeOOH.

For long-term photoelectrochemical stability experiments, the working electrode was placed < 1 cm from the liquid surface and the electrolyte was replenished as necessary to

maintain the liquid level. Illumination was provided with an ELH-type tungsten-halogen lamp and was calibrated to an equivalent power density of 100 mW cm^{-2} using a calibrated Si photodiode (Thorlabs). Photoelectrochemical stability was evaluated by cycling the electrode between day and night intervals within a 24 h period. Day cycles involved 6 h of continuous water oxidation under 100 mW cm^{-2} of simulated solar illumination at either 1.63 V vs RHE in KOH or at 1.73 V vs RHE in K-Bi, to ensure that the light-limited photocurrent density was reached in each case. Prior to each day cycle, the photoelectrodes were cycled between 0.63 V and either 1.63 V or 1.73 V vs RHE in KOH(aq) and K-Bi(aq), respectively, at 40 mV s^{-1}. Night cycles involved holding the photoelectrode at open circuit in the dark for 18 h.

Material characterization

Scanning electron microscopy (SEM) was performed using a FEI Nova NanoSEM 450 with accelerating voltages of 10 kV and a working distance of 5.0 mm. Energy-dispersive X-ray spectroscopy (EDS) was performed at accelerating voltages of 15 kV. Atomic force microscopy (AFM) was performed using a ScanAsyst-Air probe (Bruker) with a nominal tip radius of 2 nm in a Bruker Dimension Icon AFM using Peak Force Tapping mode. The Peak Force amplitude and frequency were set to 100 nm and 2 kHz, respectively. The image was measured using the software Nanoscope v9.7 and was analyzed using Nanoscope Analysis v1.9.

X-ray photoelectron spectroscopy (XPS) was performed using a Kratos Axis Ultra system at a base pressure of 1 x 10^{-9} Torr. Samples were irradiated with a monochromatic Al Kα source using X-rays (1486.7 eV) at 450 W. A hemispherical analyzer oriented for detection along the sample surface normal was used to maximize the depth sensitivity. High-resolution spectra were acquired at a resolution of 25 meV with a pass energy of 10 eV. CasaXPS computer software was used to analyze the XPS data. The spectra were first calibrated by referencing the C

1s peak position to 284.8 eV, followed by peak fitting for Ni 2p$_{3/2}$ to Ni subspecies.[34, 36] For

simplicity, satellite and Ni 2p$_{1/2}$ peaks of each subspecies were not used in peak fitting.[6] The

same peak width was used in all samples for a particular species. The XPS data were measured

ex-situ, which could potentially confound surface composition and oxidation states relative to

those in the electrochemical measurements.

Inductively coupled plasma mass spectrometry (ICP-MS) data were collected using an

Agilent 8800 Triple Quadrupole ICP-MS system to measure the extent of Si dissolution in 0.5 M

K-Bi either at open circuit or at 1.63 V vs RHE. To ensure that Si dissolution did not result from

the borosilicate glass in the electrochemical cell, reference electrode, or working electrode,

polypropylene and Teflon were used instead. ICP-MS samples were collected periodically by

removing 1 mL of solution at set time intervals. Before analysis, samples were diluted by a factor

of 10 with 2% nitric acid. ICP-MS concentration standards were made by serial dilutions with

2% nitric acid of a known concentration standard (Sigma-Aldrich). ICP-MS measurements were

conducted using hydrogen as a reaction gas to eliminate interference due to atmospheric nitrogen

in the measurement of Si. The total amount of dissolved Si from the electrodes was then

calculated and normalized to the geometric electrode area.

Figures:
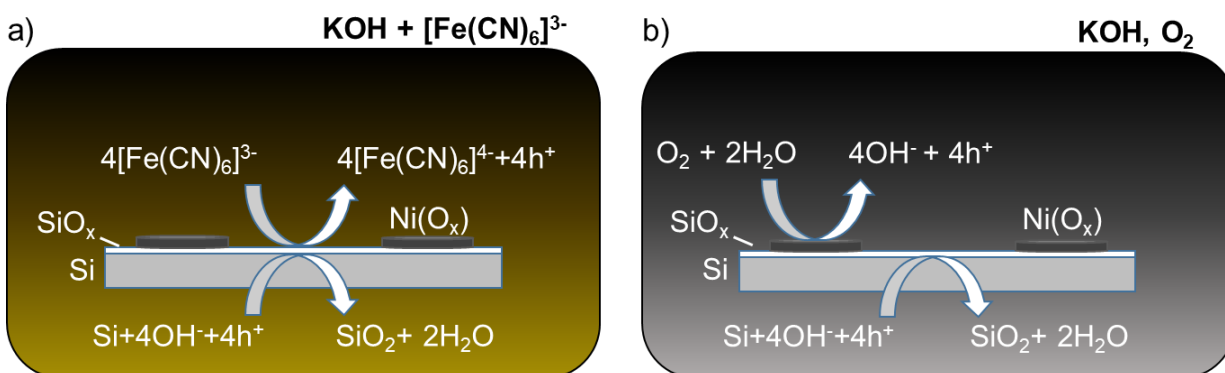
Scheme I. Schematic of two Si passivation mechanisms for a Si anode decorated with $Ni(O_x)$ islands in alkaline electrolyte at open circuit in the dark. (a) $[Fe(CN)_6]^{3-}$ is introduced as a protective electrolyte and acts as an oxidizing agent for Si.[17] (b) $Ni(O_x)$ uptakes O_2 and catalyzes Si passivation. The electrode potential shifts positive, permitting holes from the Si valence band to react with the electrolyte and oxidize Si to SiO_2.
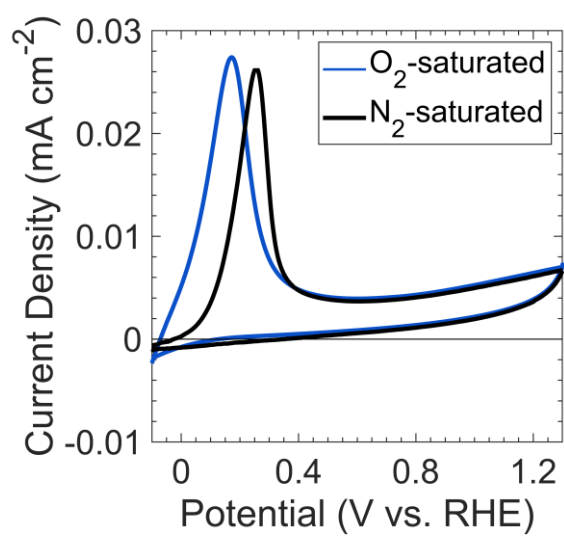
Figure 1. Cyclic voltammograms of p$^+$-Si in O$_2$- (blue) and N$_2$- (black) saturated, 1 M KOH(aq) at a 1 mV s^{-1} scan rate in the dark.
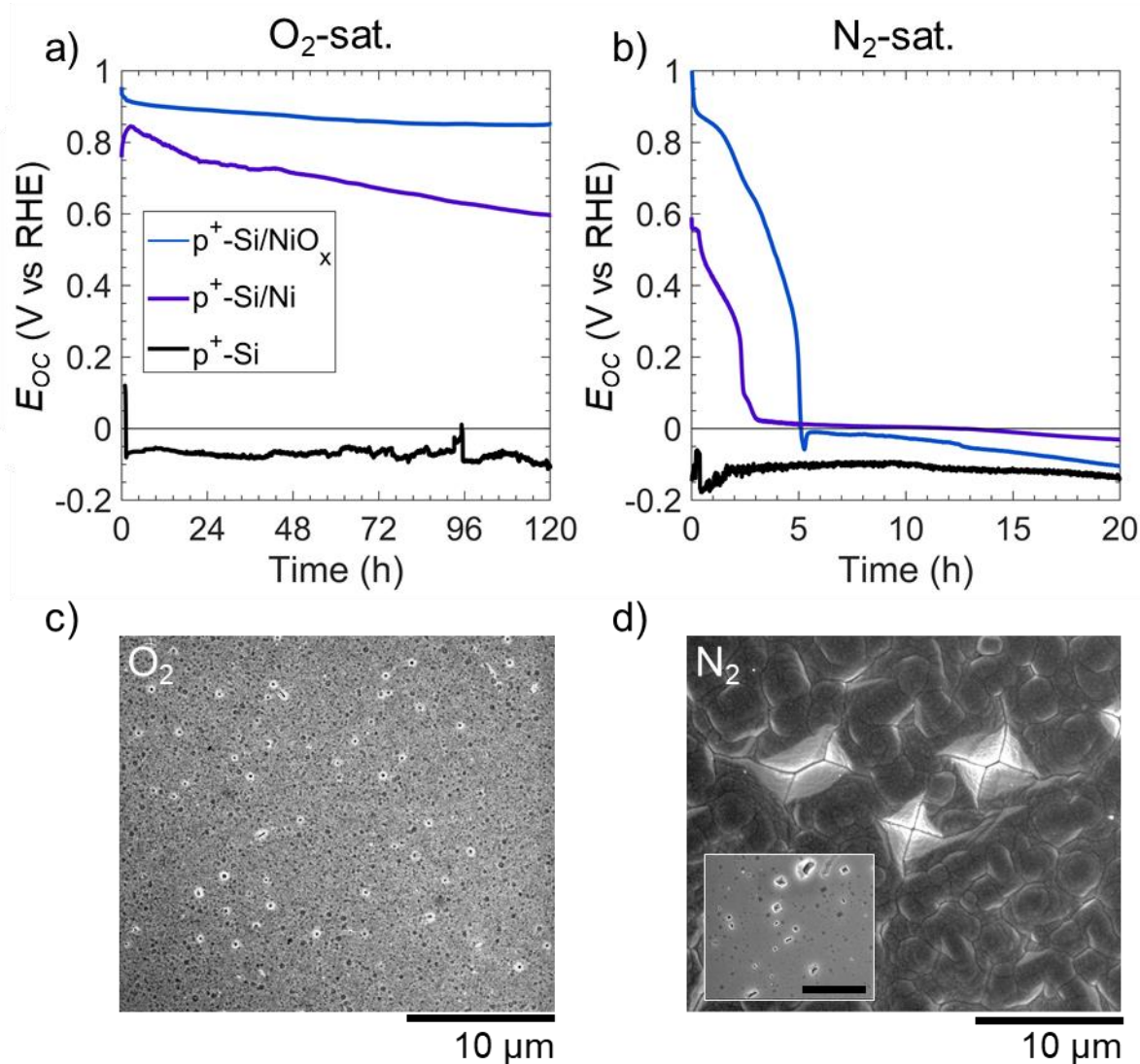
Figure 2. (a-b) Open-circuit potential (E_{oc}) vs time in the dark of p⁺-Si(100) (black), p⁺-Si(100)/Ni (purple), and p⁺-Si(100)/NiOₓ (blue) electrodes in contact with (a) O₂- and (b) N₂-saturated 1 M KOH(aq). Ni and NiOₓ thin films were 5 nm and 60 nm thick, respectively. (c-d) Scanning electron micrographs of p⁺-Si(100)/Ni electrodes after immersion for 120 h in (c) O₂-saturated and (d) N₂-saturated 1 M KOH(aq). Energy-dispersive X-ray spectroscopy confirmed that Ni was no longer on the surface on (d). Inset in (d) shows p⁺-Si/Ni after immersion in N₂-saturated KOH for 20 h, with the scale bar at 10 μm.
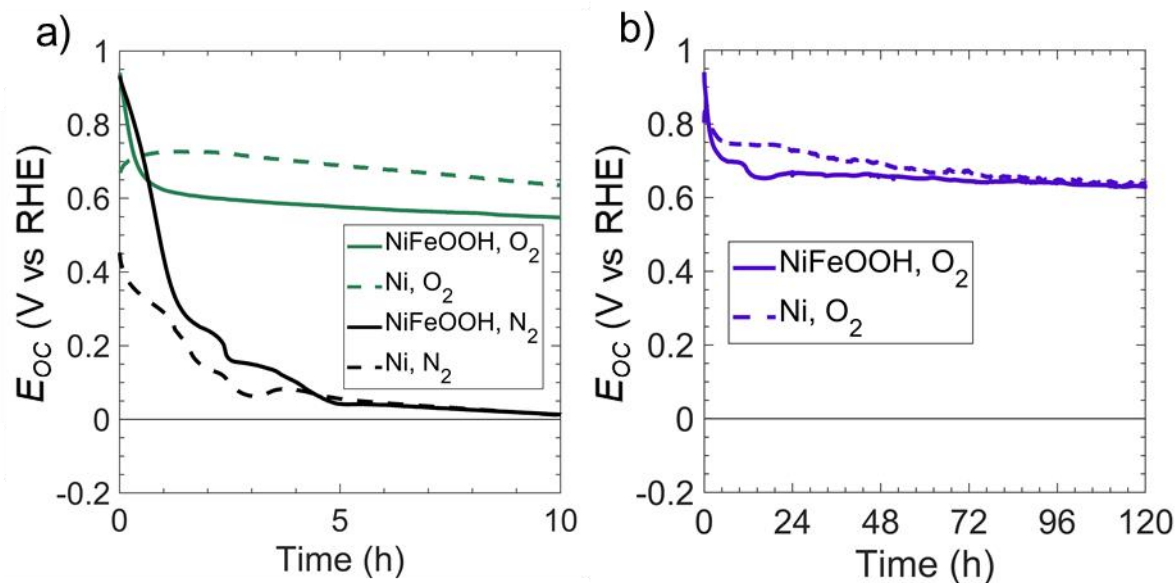
Figure 3. Comparison of the dark E_{oc} vs time behavior of p$^+$-Si/Ni electrodes in 1 M KOH(aq) with and without initial cycling of the catalyst. (a) Open-circuit potential of 3 nm thick Ni films with (solid line) and without (dashed line) cycling in O_2 (green) or N_2 (black) saturated solution over a short time period. (b) Open-circuit potential of 30 nm thick Ni films over an extended time period. Cycled films had a potential applied over 20 cycles between 0.63 and 1.63 V vs RHE at 40 mV s^{-1} to convert Ni to NiFeOOH.
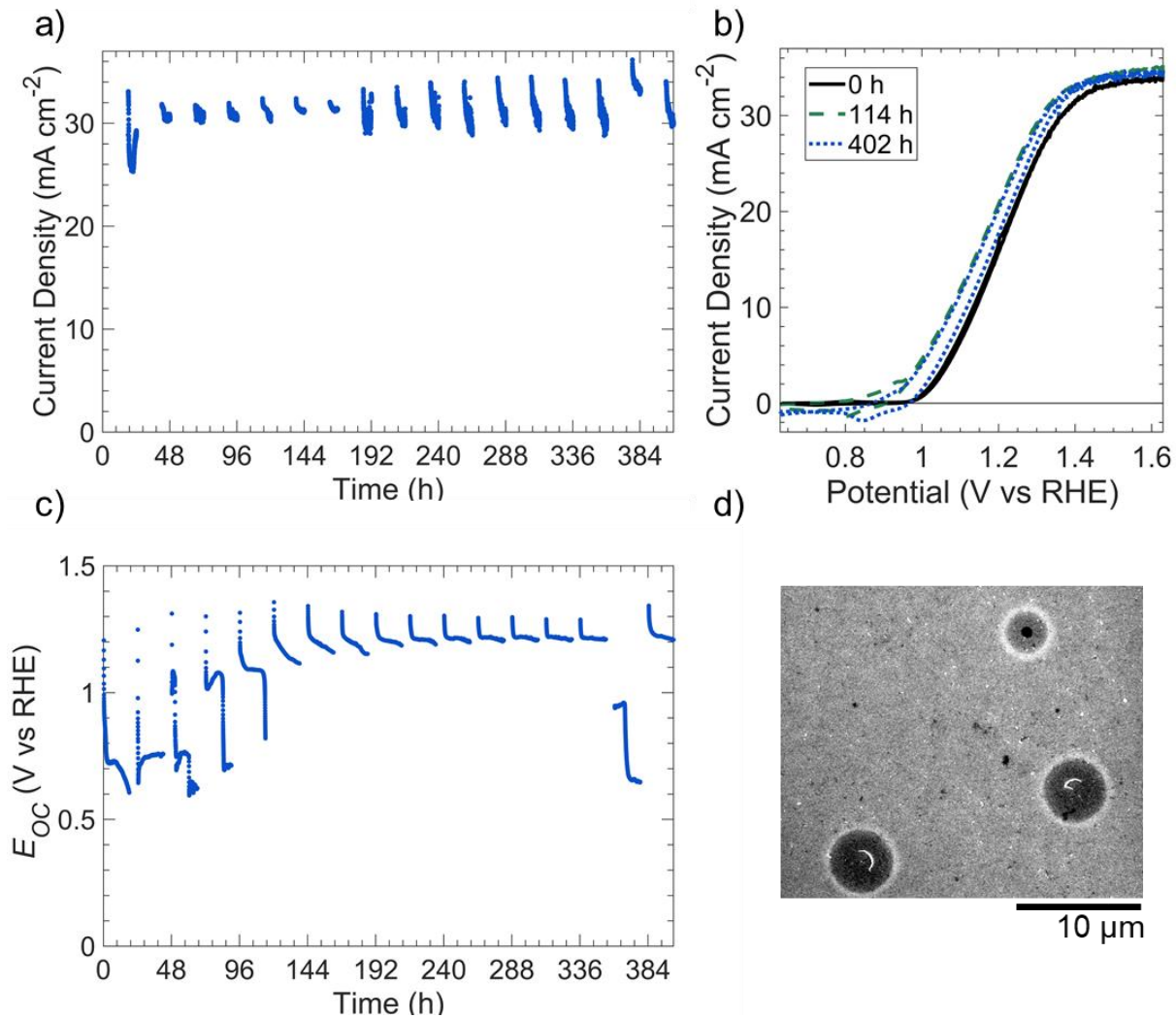
Figure 4. Stability and performance of np+-Si(100)/NiOx photoelectrodes subjected to cycling between simulated day and night conditions in 1 M KOH(aq). The deposited thickness of NiOx was 60 nm. (a) Chronoamperometric stability in 1 M KOH(aq) at 1.63 V vs RHE. (b) Cyclic voltammetry of electrode under simulated 1 sun illumination at 0 h (black, solid line), 114 h (green, dashed line), and 402 h of testing (blue, dotted line). The voltammetric scan rate was 40 mV s^{-1}. For (a-b), photoelectrodes were measured for 6 h intervals under simulated 100 mW cm^{-2} of illumination provided by an ELH-type W-halogen lamp. (c) Open-circuit potentials of the photoelectrode in the dark for 18 h intervals. The electrolyte was replenished at 168 h and 378 h to account for evaporation. (d) Scanning electron micrographs of photoelectrodes after the stability test.
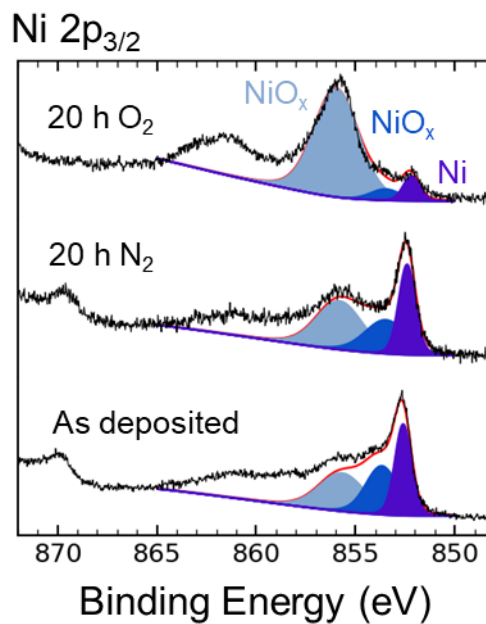
Figure 5. X-ray photoelectron spectroscopic data in the Ni 2p$_{3/2}$ region of p$^+$-Si/Ni (5 nm thick) electrodes. Electrodes were measured as deposited and after 20 h at open circuit in either N$_2$- or O$_2$-saturated 1 M KOH(aq). Ni 2p$_{3/2}$ emission was fitted with three peaks. The lowest energy peak at 852.4 eV (purple) is ascribable to Ni metal, and the higher energy peaks (blue and light blue) are assigned to NiO and Ni(OH)$_2$. The y-axis is in arbitrary units.
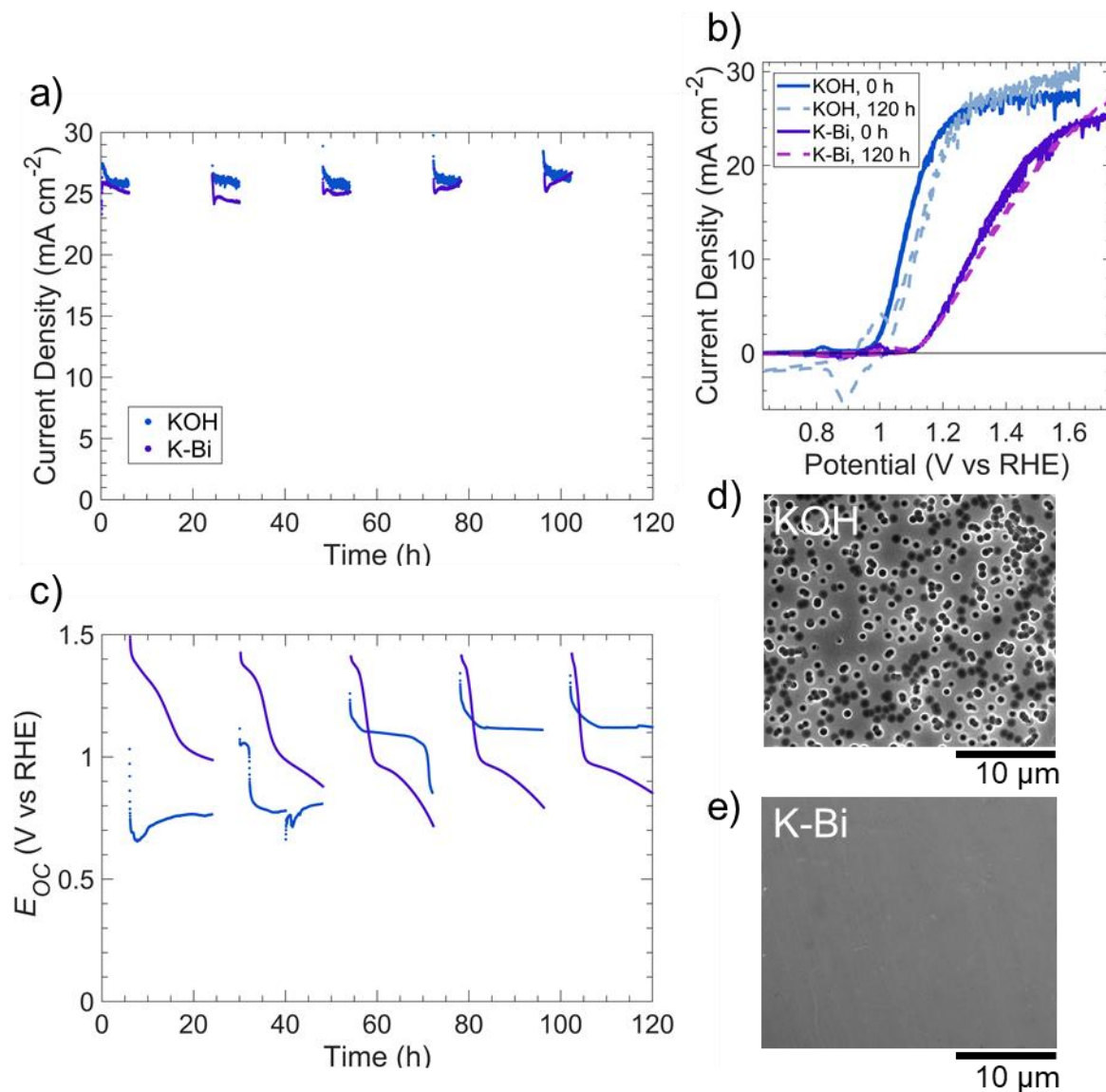
Figure 6. Comparison of the performance of np$^+$-Si(100)/Ni (5 nm) photoelectrodes and of the etching behavior at strongly alkaline pH (1 M KOH(aq)) vs near-neutral pH (0.5 M K-Bi(aq)) for electrodes subjected to cycling between simulated day and night conditions. (a) Chronoamperometric stability in 1 M KOH(aq) (blue) at 1.63 V vs RHE and 0.5 M K-Bi(aq) (purple) at 1.73 V vs RHE. (b) Cyclic voltammetry before (solid line) and after 120 h of testing (dashed line). The voltammograms scan rate was 40 mV s^{-1}. For (a-b), photoelectrodes were under 100 mW cm^{-2} of illumination provided by an ELH-type W-halogen lamp for 6 h intervals, followed by collection of (c) open-circuit potentials of the photoelectrodes for 18 h intervals in the dark. (d-e) Scanning electron micrographs of photoelectrodes after stability tests in (d) 1 M KOH(aq) and (e) 0.5 M K-Bi(aq).

References

1. M. X. Tan, P. E. Laibinis, S. T. Nguyen, J. M. Kesselman, C. E. Stanton and N. S. Lewis, in *Progress in Inorganic Chemistry*, 1994, pp. 21-144.
2. D. Bae, B. Seger, P. C. Vesborg, O. Hansen and I. Chorkendorff, *Chem Soc Rev*, 2017, **46**, 1933-1954.
3. S. Hu, M. R. Shaner, J. A. Beardslee, M. Lichterman, B. S. Brunschwig and N. S. Lewis, *Science*, 2014, **344**, 1005-1009.
4. M. J. Kenney, M. Gong, Y. Li, J. Z. Wu, J. Feng, M. Lanza and H. Dai, *Science*, 2013, **342**, 836-840.
5. K. Sun, M. T. McDowell, A. C. Nielander, S. Hu, M. R. Shaner, F. Yang, B. S. Brunschwig and N. S. Lewis, *The Journal of Physical Chemistry Letters*, 2015, **6**, 592-598.
6. K. Sun, F. H. Saadi, M. F. Lichterman, W. G. Hale, H. P. Wang, X. Zhou, N. T. Plymale, S. T. Omelchenko, J. H. He, K. M. Papadantonakis, B. S. Brunschwig and N. S. Lewis, *Proc Natl Acad Sci U S A*, 2015, **112**, 3612-3617.
7. X. Zhou, R. Liu, K. Sun, D. Friedrich, M. T. McDowell, F. Yang, S. T. Omelchenko, F. H. Saadi, A. C. Nielander, S. Yalamanchili, K. M. Papadantonakis, B. S. Brunschwig and N. S. Lewis, *Energy & Environmental Science*, 2015, **8**, 2644-2649.
8. X. Zhou, R. Liu, K. Sun, K. M. Papadantonakis, B. S. Brunschwig and N. S. Lewis, *Energy & Environmental Science*, 2016, **9**, 892-897.
9. P. Buabthong, Z. P. Ifkovits, P. A. Kempler, Y. Chen, P. D. Nunez, B. S. Brunschwig, K. M. Papadantonakis and N. S. Lewis, *Energy & Environmental Science*, 2020, **13**, 4269-4279.
10. D. Bae, S. Shayestehaminzadeh, E. B. Thorsteinsson, T. Pedersen, O. Hansen, B. Seger, P. C. K. Vesborg, S. Ólafsson and I. Chorkendorff, *Sol. Energy Mater. Sol. Cells*, 2016, **144**, 758-765.
11. M. R. Shaner, S. Hu, K. Sun and N. S. Lewis, *Energy & Environmental Science*, 2015, **8**, 203-207.
12. H. G. G. Philipsen and J. J. Kelly, *The Journal of Physical Chemistry B*, 2005, **109**, 17245-17253.
13. K. Sun, Nicole L. Ritzert, J. John, H. Tan, W. G. Hale, J. Jiang, I. Moreno-Hernandez, K. M. Papadantonakis, T. P. Moffat, B. S. Brunschwig and N. S. Lewis, *Sustainable Energy & Fuels*, 2018, **2**, 983-998.
14. K. Oh, C. Mériadec, B. Lassalle-Kaiser, V. Dorcet, B. Fabre, S. Ababou-Girard, L. Joanny, F. Gouttefangeas and G. Loget, *Energy & Environmental Science*, 2018, **11**, 2590-2599.
15. P. M. M. C. Bressers, S. A. S. P. Pagano and J. J. Kelly, *Journal of Electroanalytical Chemistry*, 1995, **391**, 159-168.
16. X. H. Xia and J. J. Kelly, *Electrochimica Acta*, 2000, **45**, 4645-4653.
17. H. J. Fu, I. A. Moreno-Hernandez, P. Buabthong, K. M. Papadantonakis, B. S. Brunschwig and N. S. Lewis, *Energy & Environmental Science*, 2020, **13**, 4132-4141.
18. D. R. Lide, *CRC handbook of chemistry and physics*, CRC press, 2004.
19. P. M. M. C. Bressers, J. J. Kelly, J. G. E. Gardeniers and M. Elwenspoek, *J. Electrochem. Soc.*, 1996, **143**, 1744-1750.
20. O. J. Glembocki, R. E. Stahlbush and M. Tomkiewicz, *Journal of The Electrochemical Society*, 1985, **132**, 145-151.

21.   J. W. Faust and E. D. Palik, *Journal of The Electrochemical Society*, 1983, **130**, 1413-1420.
22.   W. A. Pliskin and H. S. Lehman, *Journal of The Electrochemical Society*, 1965, **112**, 1013-1019.
23.   P. Allongue, V. Costa-Kieling and H. Gerischer, *Journal of The Electrochemical Society*, 1993, **140**, 1018.
24.   L.-A. Stern and X. Hu, *Faraday Discussions*, 2014, **176**, 363-379.
25.   L. Trotochaud, S. L. Young, J. K. Ranney and S. W. Boettcher, *Journal of the American Chemical Society*, 2014, **136**, 6744-6753.
26.   L. F. Huang, M. J. Hutchison, R. J. Santucci, J. R. Scully and J. M. Rondinelli, *The Journal of Physical Chemistry C*, 2017, **121**, 9782-9789.
27.   O. Diaz-Morales, D. Ferrus-Suspedra and M. T. M. Koper, *Chemical Science*, 2016, **7**, 2639-2645.
28.   M. Hannula, H. Ali-Löytty, K. Lahtonen, E. Sarlin, J. Saari and M. Valden, *Chemistry of materials : a publication of the American Chemical Society*, 2018, **30**, 1199-1208.
29.   S. Sui, X. Wang, X. Zhou, Y. Su, S. Riffat and C.-j. Liu, *Journal of Materials Chemistry A*, 2017, **5**, 1808-1825.
30.   P. Yin, T. Yao, Y. Wu, L. Zheng, Y. Lin, W. Liu, H. Ju, J. Zhu, X. Hong, Z. Deng, G. Zhou, S. Wei and Y. Li, *Angewandte Chemie International Edition*, 2016, **55**, 10800-10805.
31.   H. Abroshan, P. Bothra, S. Back, A. Kulkarni, J. K. Nørskov and S. Siahrostami, *The Journal of Physical Chemistry C*, 2018, **122**, 4783-4791.
32.   A. Andersson, W. Estrada, C.-G. Granqvist, A. Gorenstein and F. Decker, *Characterization of electrochromic dc-sputtered nickel-oxide-based films*, SPIE, 1990.
33.   D. S. Jensen, S. S. Kanyal, N. Madaan, M. A. Vail, A. E. Dadson, M. H. Engelhard and M. R. Linford, *Surface Science Spectra*, 2013, **20**, 36-42.
34.   M. C. Biesinger, B. P. Payne, L. W. M. Lau, A. Gerson and R. S. C. Smart, *Surface and Interface Analysis*, 2009, **41**, 324-332.
35.   M. C. Biesinger, B. P. Payne, A. P. Grosvenor, L. W. M. Lau, A. R. Gerson and R. S. C. Smart, *Applied Surface Science*, 2011, **257**, 2717-2730.
36.   A. P. Grosvenor, M. C. Biesinger, R. S. C. Smart and N. S. McIntyre, *Surface Science*, 2006, **600**, 1771.
37.   M. R. Singh, K. Papadantonakis, C. Xiang and N. S. Lewis, *Energy Environ. Sci*, 2015, **8**, 2760-2767.
38.   S. V. Mattigod, D. Rai, A. R. Felmy and L. Rao, *Journal of Solution Chemistry*, 1997, **26**, 391-403.
39.   L. Smardz, U. Köbler and W. Zinn, *Journal of Applied Physics*, 1992, **71**, 5199-5204.
40.   P. Nunez, M. H. Richter, B. D. Piercy, C. W. Roske, M. Cabán-Acevedo, M. D. Losego, S. J. Konezny, D. J. Fermin, S. Hu, B. S. Brunschwig and N. S. Lewis, *The Journal of Physical Chemistry C*, 2019, **123**, 20116-20129.
41.   M. H. Richter, W.-H. Cheng, E. J. Crumlin, W. S. Drisdell, H. A. Atwater, D. Schmeißer, N. S. Lewis and B. S. Brunschwig, *Chemistry of Materials*, 2021, **33**, 1265-1275.
42.   K. Sun, R. Liu, Y. Chen, E. Verlage, N. S. Lewis and C. Xiang, *Advanced Energy Materials*, 2016, **6**.
43.   S. Hu, N. S. Lewis, J. W. Ager, J. Yang, J. R. McKone and N. C. Strandwitz, *The Journal of Physical Chemistry C*, 2015, **119**, 24201-24228.